

Studies in Astronomical Time Series Analysis: The Double Lomb-Scargle Periodogram and Super Resolution

JEFFREY D. SCARGLE¹ AND SARAH WAGNER^{2, 3, 4}

¹ *Astrobiology and Space Science Division (retired), NASA Ames Research Center, Moffett Field, CA 94035, USA*
jeffscargle@gmail.com

² *Julius-Maximilians-Universität Würzburg, Fakultät für Physik und Astronomie, Institut für Theoretische Physik und Astrophysik, Lehrstuhl für Astronomie, Emil-Fischer-Str. 31, D-97074 Würzburg, Germany*

³ *Kavli Institute for Particle Astrophysics and Cosmology and SLAC National Accelerator Laboratory, Stanford University, Menlo Park, California 94025, USA*

⁴ *Institut de Física d'Altes Energies (IFAE), The Barcelona Institute of Science and Technology (BIST), E-08193 Bellaterra (Barcelona), Spain*

Submitted to ApJL

ABSTRACT

Multiple-frequency periodograms – based on time series models consisting of two or more independent sinusoids – have long been discussed. What is new here is the presentation of a practical, simple-to-use computational framework implementing this concept. Our algorithms have super resolution that evades the Rayleigh criterion, as well as provision for statistical weighting and tapering. They can be used for essentially any time series (e.g. time-tagged events or point measurements) with arbitrary sampling – even or uneven. Examples of super resolution of synthetic data, sunspot numbers, and the rich pulsations of white dwarf J0135+5722, demonstrate practical applications. Appendices derive generalized periodograms using an arbitrary number of arbitrary basis functions (following Bretthorst, 1988) and define several examples of non-sinusoidal bases for these “omnigrams”. Application beyond the frequency domain is demonstrated with an autoregressive model exhibiting super resolution in the time domain. A GitHub repository containing omnigram code, and symbolic algebra scripts for generating it, will soon be available.

Keywords: Time Series Analysis, Lomb-Scargle Periodogram, Rayleigh Criterion, Multi-periodic Pulsation, Data Analysis, Sunspot Numbers, Pulsating White Dwarfs, Periodograms, Omnimograms

1. THE HUNT FOR PERIODICITY

Oscillation, rotation, revolution, and wave propagation are common, relatively straightforward, physical processes associated with periodic variability – a signature relatively easy to detect, characterize and interpret. Hence study of known and suspected periodicities in noisy data is a major task of astronomical time series analysis.

The *periodogram* is the workhorse tool in the hunt for periodic signals and characterizing them when detected. This term was coined by Schuster (1898) for his estimator of the true or theoretical *power spectrum* of a process. Currently several other estimators are in use, e.g. likelihood profiles and Fourier transforms of autocorrelation functions. Here we discuss four different power spectrum estimators: namely maximum likelihood and marginalized posterior variants of the Schuster and Lomb-Scargle periodograms.

These hunting expeditions are made difficult by a number of well-known obstacles: the periodogram is inherently noisy, and in a way that does not automatically improve with more data. Spectral leakage – power appearing at the wrong frequency – is always present in one degree or another. To address these problems, various smoothing, filtering, averaging, tapering, or other time and/or frequency domain processing steps are routinely invoked, followed by attempts to account for the resulting modification of the underlying signal.

Interpretation of a power spectrum estimate, once obtained, faces further difficulties. Non-periodic low-frequency behavior of many astrophysical sources tends to generate periodogram peaks that may seduce the eager period hunter. The wider net of the hunt for quasi-periodic oscillations (QPOs) invites even more impersonation of spectral features by statistical fluctuations. Especially, but not exclusively, for unevenly sampled data the window function can substantially affect the periodogram in a way that is not easy to account for.

Determining the “significance” of claimed periodicities is a minefield that few traverse unscathed. Fundamental are the classic concepts of *statistical significance*, rooted in the theory of *analysis of variance*, but complicated by known and unknown systematic errors and selection effects, correlated non-Gaussian errors of observation, and especially the presence of aperiodic variability intrinsic to the source but unrelated to periodicities (e.g. [Vaughan 2010](#)). These effects result in any potential periodicity being superposed on a confusing mix of two kinds of random non-white “noise” – for example leading to uncertainty in the crucial area of possible periodic signals from black hole systems, summarized by [Molina et al. \(2001\)](#).

On the other hand, in practice, larger uncertainty in assessing the substantive importance of putative spectral features typically arises from subjective issues: e.g. determining how to evaluate *trials factors* to account for the number of “cases” inspected, clear specification of assumptions, prior specification of “what would be considered interesting” in exploratory data analysis, and unambiguous setting of hypotheses in post-exploratory data analysis. If all of these issues are not addressed fully and correctly – an effort discouraged by uncritical reliance on automated analysis tools – spurious discovery claims may result. The conclusion that only features so strong as to be obvious in visual inspection of the periodogram can be considered reliably detected, is perhaps not too extreme.

We do not address significance issues here, other than to note that applications of generalized periodograms will face all of the same difficult problems. Trial factors problems will be worsened by the multi-frequency nature of the tools, but should involve the same conceptual issues.

2. THE LOMB-SCARGLE PERIODOGRAM

The *Lomb-Scargle periodogram* (LSP) algorithm is in wide use for analysis of unevenly sampled time series. Without reviewing the entire history, it is worth mentioning that [Barning \(1963\)](#) defined the same multi-frequency model central to the present work, and presented an algorithm for what should perhaps be known as the *Barning-Lomb-Scargle periodogram*. [Bretthorst \(2000\)](#) elevated the LSP from its status as least-squares fitting of sinusoids into a rigorous Bayesian framework. He framed determining the frequency of a single sinusoid in noisy data as a Bayesian parameter estimation problem. He showed that the LSP is “the sufficient statistic for single frequency estimation in a wide class of problems.” Specifically, this periodogram can be obtained from the likelihood for a model consisting of a single sinusoid, and data with independent Gaussian measurement errors. This error model is fundamental to the formulation and derivation of periodograms in Bretthorst’s and our analysis; in both, the procedure is to marginalize this Gaussian likelihood over all its parameters (amplitude and phase) except frequency. As a result, the full posterior $P(\omega)$ is available, allowing peak hunters to focus on finding maxima – “bump hunting” in the periodogram – as well as assessing uncertainty in the period.

[Mortier et al. \(2015\)](#) developed a generalized periodogram in the Bayesian setting ([Bretthorst 2000](#)), using the Gaussian integral Eq. (C.2), much as we do in Appendix C, to generate an explicit algorithm, the Bayesian generalized Lomb-Scargle periodogram (BGLS). [VanderPlas \(2018\)](#) overviewed a number of practical issues. Other general treatments include [Vio, Andreani and Biggs \(2010\)](#); [Olspt, Pelt and Käpylä \(2018\)](#); [Lenoir and Crucifix \(2018\)](#).

2.1. Generalizations

Bretthorst’s pioneering work included a number of important generalizations, such as non-sinusoidal and amplitude-modulated signals ([Bretthorst 2001a,b, 2003, 2008](#)). Between these and many other modifications, the term *Generalized-Lomb-Scargle Periodogram* is ambiguous. In the most common usage GLSP seems to refer to inclusion of an additive constant (e.g. [Zechmeister and Kürster 2009](#), and earlier work), apparently inspired by problems with subtracting a mean determined in pre-processing. we see these anecdotal considerations, but raise an opposing one: for sunspot number data, [Bretthorst \(1988\)](#) computed marginalized posterior periodograms as described at the beginning of this section. He found only a trivial difference, at zero frequency, between modeling an additive constant and pre-subtracting an externally determined value. The theoretical preferability of the former, especially for estimating uncertainties, may be outweighed by various practical considerations, such as availability of reliable ancillary information about a background constant.

2.2. Criticisms

Because the double periodogram described here inherits properties from the LSP – for better or worse – a discussion of its properties and limitations is in order. Critiques in the literature are numerous; here we comment on a few issues, including criticisms, misunderstandings and misuses of the algorithm.

It is frequently assumed, often implicitly, that the LSP somehow corrects for uneven sampling. It does not. It simply allows the computation of a useful statistical function for arbitrarily spaced measurements. It is left to the user to address sampling effects, the most important of which center around a few related issues: lack of a well defined Nyquist frequency, complicated window functions, aliasing and other spectral leakage – problems which are said to worsen as the sampling becomes more irregular. In many settings (Dawson and Fabrycky 2010, e.g.) uneven sampling breaks the relations underlying aliasing, resulting in a beneficial reduction of this form of leakage. Further, the user is free to explore corrections for the irregularity in sampling, e.g. deconvolving the window function¹ in post-processing.

A common pitfall arises in determining false-positive rates in a background of colored noise, a setting in which the classic exponential probability distribution of the periodogram in white noise is invalid. It is sometimes claimed that the LSP can only be used if the noise is white. While it is true that the derivation of LSP assumes independent Gaussian residuals, in practice it has proven useful more generally. It is said that the LSP does not include weights, although Gilliland and Baliunas (1987) gave a prescription for applying weights, as did Scargle (1989) (which also gives an algorithm for the complex Fourier transform of data with arbitrary sampling, useful in its own right and for computing not just periodograms, but also cross-correlations, cross-spectra, co-spectra, etc.) As demonstrated in Appendices A and D, statistical weights apply to all summations in the periodogram formula, including the trigonometric terms not involving x_n . Tapers are deterministic modulations of the time series, not statistical weights, and ordinarily would apply to x_n only.

The criticism directly motivating the current paper is that *a periodogram based on a model consisting of a single sinusoid is not applicable to more complicated signals*, such as multiple sinusoids of different frequencies, periodic but non-sinusoidal signals, or processes with continuous spectra, such as quasi-periodic oscillations or $1/f$ -noise – in short anything other than a single pure sine wave. This criticism is clearly justified as a matter of principle, but we do not know of any articulation of specific problems associated with it. In practice, periodograms are routinely and uncritically taken to serve as general purpose spectral estimators. In this paper we address one element of this question, by providing explicit algorithms for periodograms based on a model consisting of the sum of two independent sinusoidal signals, with different frequencies, phases, and amplitudes.

3. DOUBLE PERIODOGRAMS

Having been around for over 60 years, the notion of multi-frequency periodograms is hardly new. Barnard (1963) formulated this issue and described an iterative, expectation-maximization-like approach; Lomb (1976) focused on correlations between residuals from a two-sinusoid model. Most relevant here, in a comprehensive study of both theoretical and practical aspects of power spectrum analysis from a Bayesian point of view, Bretthorst (1988) developed generalized periodograms for non-sinusoidal, and amplitude-modulated signals, using basis functions with an arbitrary number of components at different frequencies. From a model consisting of a linear combination of arbitrary, perhaps not even orthogonal, basis functions, he developed a variety of specialized periodograms – e.g. for sinusoids, decaying sinusoids, and chirps. More recent discussions of the concept of multi-frequency periodograms include (Baluev 2013a,b, 2015; Seilmayer, Wondrak, and Garcia 2025). Loredo (2001) explored multiple periodograms in an acoustics context.

We have developed explicit algorithms that are neither special cases nor generalizations of these developments, but simply implementations of them. Appendices utilize Bretthorst's formalism and notation to produce more general algorithms, but here we start with the model for the signal y_n , in notation adopted in essentially all of previous work: the sum of two sinusoids of circular frequencies ω_1 and ω_2 (radians per unit time):

$$y_n = a_1 \cos(\omega_1 t_n - \theta_1) + b_1 \sin(\omega_1 t_n - \theta_1) + a_2 \cos(\omega_2 t_n - \theta_2) + b_2 \sin(\omega_2 t_n - \theta_2), \quad (1)$$

where the t_n are the times of measurement, and a_1, b_1, a_2, b_2 are amplitude parameters. The θ s are optional Lomb phase parameters, here used in the same way as for the LSP as will be described below.

¹ E.g. evaluated as the periodogram of a synthetic sinusoid, at the frequency of interest, sampled at the same times as the actual data.

Specification of the model for the errors σ_n in the x_n measured at times t_n completes the definition of the likelihood. Taking measurement errors to be independently and normally distributed gives the standard Gaussian log-likelihood:

$$\log L = -\frac{1}{2} \sum_{n=1}^N \left(\frac{x_n - y_n}{\sigma_n} \right)^2, \quad (2)$$

The values of σ_n are readily incorporated in the form of statistical weights $w_n = 1/\sigma_n^2$ individually (cf. Appendix A), or with a constant for homoskedastic errors. We assume any constant or other extraneous trend has been removed from the data, so no constant term is included. This summation can be expanded into this expression for the mean square residual:

$$\begin{aligned} \text{Resid} = & a_1^2 CC11 + b_1^2 SS11 + a_2^2 CC22 + b_2^2 SS22 \\ & - 2(a_1 XC1 + b_1 XS1 + a_2 XC2 + b_2 XS2) \\ & + 2(a_1 b_1 CS11 + a_1 a_2 CC12 + a_1 b_2 CS12 \\ & + b_1 a_2 SC12 + b_1 b_2 SS12 + a_2 b_2 CS22) \end{aligned} \quad (3)$$

Here the coefficients of the amplitude parameters are weighted summations over n of the cross products in the resulting quadratic form, as given in several of the references cited above. Referring to Eq. (1), the letters C and S indicate the cos and sin terms, indices indicating which of the two components is involved, and X refers to a data term. For example $CS12 = \sum w_n \cos(\omega_1 t_n - \theta_1) \sin(\omega_2 t_n - \theta_2)$ and $XC1 = \sum w_n x_n \cos(\omega_1 t_n - \theta_1)$. The Lomb procedure orthogonalizing the sin and cos basis functions, for each frequency separately, can be implemented simply by omitting the corresponding terms, $CS11$ and $CS22$. See Appendix E for details.

In addition, we provide automated tools for generating related algorithms for models of arbitrary order.

For the full expression, refer to the appendix where this is all written out, and in a more organized notation that emphasizes the great generality – an arbitrary number of basis functions, not just sin and cos – hidden in the formulas here. There are two types of periodograms are described, based on maximizing or marginalizing the likelihood with respect to its parameters a_1, b_1, a_2, b_2 . For each of these two variants result depending on whether or not one invokes Lomb's procedure of orthogonalizing $\cos(\omega_1 t_n - \theta_1)$ and $\sin(\omega_1 t_n - \theta_1)$ – and separately $\cos(\omega_2 t_n - \theta_2)$ and $\sin(\omega_2 t_n - \theta_2)$ – with respect to summation over n . Cross terms $\cos(\omega_1 t_n - \theta_1)$ and $\sin(\omega_2 t_n - \theta_2)$, etc., are never orthogonalized, as this would destroy crucial information on the interaction between the two sinusoidal components.

Automatic byproducts of the computations of the maximum likelihood periodograms are the corresponding values of the amplitude parameters (cf. Appendix B). They can also be obtained in post-processing of the marginalized likelihood periodograms. For each component these amplitudes yield estimates of the amplitudes and phases of the sinusoids.

4. SUPER RESOLUTION

Double periodograms are constructed to separate periodic signals with different frequencies. As we shall now see, they are capable of separating periodic signals whose point-spread functions overlap significantly, so that a single-frequency periodogram does not resolve them. Bretthorst (1988) discusses this issue, and some remarkable results for 1D periodograms.

This section demonstrates the remarkable feature of super resolution: *pairs of sinusoidal signals with frequencies too close to be resolved by an ordinary single periodogram can be resolved by a double periodogram*. Over an interval T , corresponding to a fundamental frequency of $\omega_0 = 2\pi/T$ radians per unit time, two sinusoids differing in frequency by $\Delta\omega$ differ in phase by $\Delta\omega T$. Thus the two components differ significantly from each other to the extent that this phase is $\gtrsim \pi$. Accordingly, we define a dimensionless *Rayleigh parameter*

$$\mathcal{R}_{\text{Rayleigh}} \equiv \Delta\omega/\omega_0 \quad (4)$$

to quantify frequency separations, and refer to the notion that $\mathcal{R}_{\text{Rayleigh}} \gtrapprox 1$ is necessary for the resolution of two spectral components as the *Rayleigh criterion*.

It is easy to think that, given a time series of length T , resolution in the frequency domain is inherently and unavoidably limited to frequencies differing by $\Delta\omega > \omega_0$, or $\mathcal{R}_{\text{Rayleigh}} > 1$. See Ramirez Delgado, Caicedo Vivas, Dodson-Robinson, and Haley (2025) for a recent overview of this concept, including discussion of iterative “cleaning” approaches to extracting multiple signals – find one and remove it; repeat – and the

possibility of spurious double peaks due to uneven sampling. *However, this criterion is not a constraint on periodicity detection in general; it applies to the use of single-frequency Fourier periodograms, and can be violated with other detection schemes.*

Double periodograms break the Rayleigh criterion because of the way optimization of Eq. (1) isolates the components. This isolation does not happen in the time domain – for both sinusoids in Eq. (1) are fit to the same data – rather in the frequency domain. The mean-square residual is diminished if both frequencies ω_1 and ω_2 match sinusoidal components in the data – just as happens with an ordinary periodogram at a single frequency. The resolving power of a multiple-frequency periodogram is limited more by signal-to-noise of the data than it is by ω_0 .

Figure 1 addresses this issue with two sinusoids sampled at the same random and uniformly distributed times, with a frequency difference of $0.3\mathcal{R}_{\text{ayleigh}}$. The DLSP recovers the input signal almost exactly. Dashed lines between the panels emphasize that slices of the DLSP through its maximum serve as individual 1D periodograms for the two sinusoids; their maxima are indistinguishable from the true values on the scale of this figure (the errors are .0002 and .0102 times the fundamental frequency). In contrast to this resolution and accurate quantification of the true separation of the two sinusoids, the LSP in the lower-righthand panel does not even present two peaks, and is thus incapable of resolving the components. The best fit amplitudes were very accurate too: 4.029 and 0.984 (true values 4 and 1).

It can be seen in the figure that this enhanced resolution does not come from super-narrow peaks in 1D slices of the 2D periodogram; in fact these are not particularly narrow, e.g. compared to the 1D LSP. Rather the two sinusoids of Eq. (1) separately model the two components, allowing their frequencies to be accurately determined by finding the maxima of these relatively broad, but smooth, curves. The phases and amplitudes can also be well determined, as we see next.

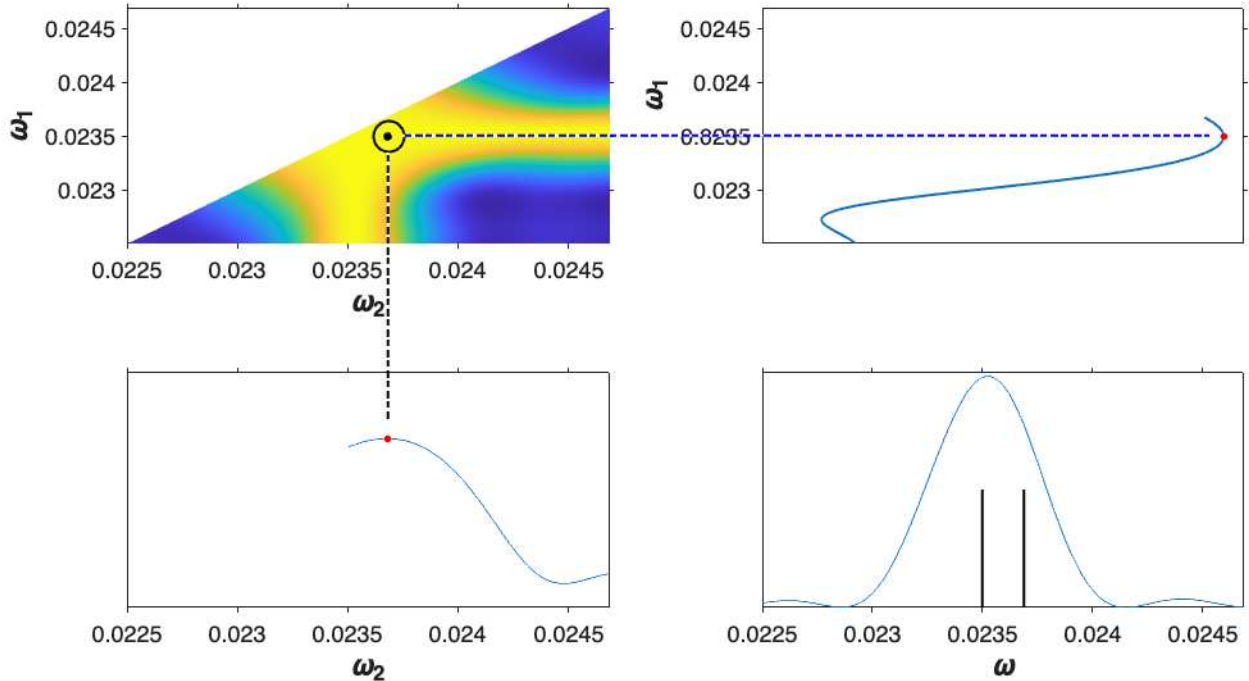


Figure 1. Resolution of two synthetic sinusoids: Upper Left: the double Lomb-Scargle periodogram $P(\omega_1, \omega_2)$ for two sinusoids of length 10000 seconds ($\omega_0 = 6.2886\text{e-}04$ radians per second) with frequencies of .0235 and .0237 radians per second (i.e. $\mathcal{R}_{\text{ayleigh}} = .3$), amplitudes 1 and 4, and with additive Gaussian noise of amplitude 0.1. The circle is centered on the true values $\omega_1 = 0.0235$ and $\omega_2 = 0.0237$; the black dot is the local maximum of $P(\omega_1, \omega_2)$, precisely recovering the true values. Values above the diagonal, redundant due to symmetry, are not shown. Upper-right and lower-left: slices of $P(\omega_1, \omega_2)$ passing through this maximum; their maxima yield frequency estimates indicated by red dots. Lower-right: the 1D LSP, with vertical lines indicating the true input frequencies.

Let's expand on the above example and elucidate the range of sinusoid frequency separations over which super resolution obtains, and how it degrades with decreasing signal-to-noise. Figure 2 explores how faithfully frequency separation is recovered, as a function of the true value and the additive noise level. This parameter is remarkably well tracked for $R \approx > 0.5$ and even smaller frequency separations as long as the noise level is not too great.

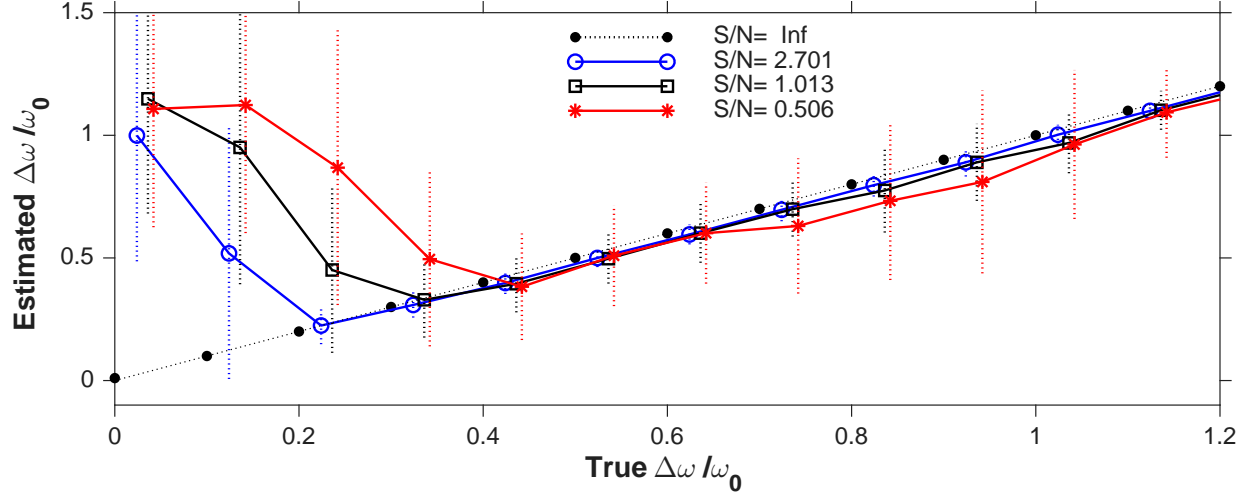


Figure 2. DLSP Super Resolution. The estimated frequency separation of two sinusoids, with four different levels of additive Gaussian noise, is plotted as a function of their true separation, in units of the fundamental. Indicated S/N values are the ratio of the sinusoid amplitude to the noise standard deviation. Abscissas are slightly offset for clarity. The points are averages, and 1σ error bars are standard deviations, of the estimated component separations over 128 realizations of the noise and time-sampling.

Our double maximum-likelihood periodogram algorithms automatically yield optimized values of the four amplitude parameters in Eq. (1), directly or with a correction for the phase shift introduced by the Lomb procedure (see the Appendix). Figure 3 demonstrates that these estimates are exact for all separations $\Delta\omega/\omega_0$ in the noise-free case, but degrade for increasing noise, especially at low separations. These results are presented as proof of the concept

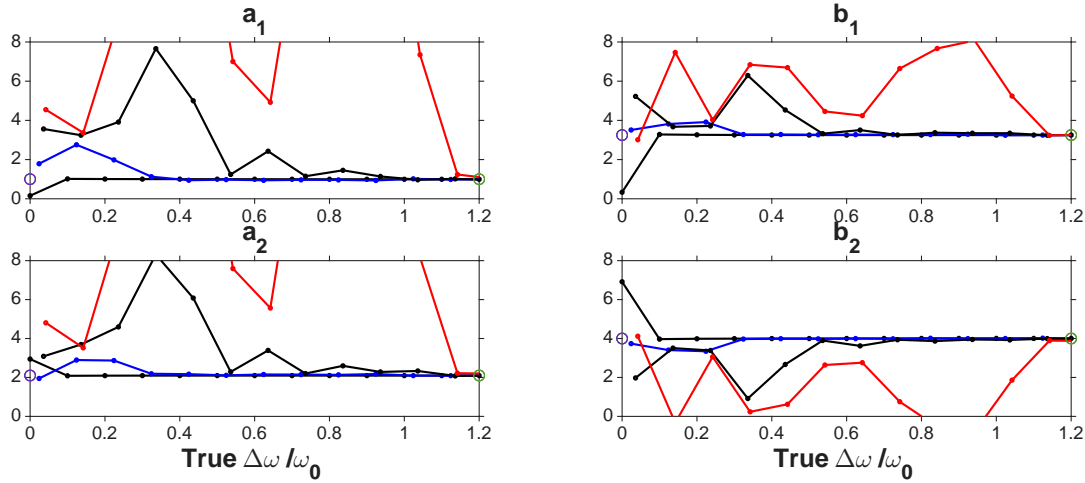


Figure 3. Recovery of Amplitudes. The estimated values of the four parameters a_1, b_1, a_2 and b_2 in Eq. 1 (from which the amplitudes and phases of the two component sinusoids can be computed) are plotted as a function of the Rayleigh parameter R . The arbitrarily chosen input values (1, 3.25, 2.1 and 4) are open circles at the ends of the range. These plots are based on the same simulation as in Fig. 2, and use the same colors to indicate the four signal-to-noise cases.

that *double periodograms can resolve periodic signals surprisingly close in frequency, and recover estimates of their amplitudes and phases*. Unlimited resolving power for large signal-to-noise should not be a surprise.

5. DOUBLE PERIODOGRAM APPLICATIONS

This section demonstrates a few things that can be accomplished using the DLSP on two astronomical time series. Other applications will no doubt occur to the reader, e.g. to asteroseismology, active galactic nuclei, exoplanets, etc.

5.1. Practical Issues

Some practical issues for ordinary periodogram analysis carry over, with some modifications, to double periodograms and higher order omnigrams. But some novel considerations and opportunities arise in the multi-frequency setting. Going to a higher dimension infinitely increases geometrical complexity, enabling innovative time series diagnostics.

A local maximum, e.g. in a 2D periodogram, still marks a possible periodicity – single if it lies on the diagonal $\omega_1 = \omega_2$, but resolved into two if offset from it. As with a 1D periodogram, after identifying such a peak it is natural to examine its profiles, i.e. slices of the periodogram through that point. Of particular interest is structure in the sidelobes of the main peak. With multiple-frequency periodograms there is a choice of orientation for these slices. In 2D, slicing parallel to the ω_1 or ω_2 axes is an obvious choice. For off-diagonal peaks, slices in both of these directions are meaningful; as we will see in the next section, these profiles exhibit information about the two detected signals. Presumably other features of these functions will be informative – e.g. saddle points, profiles along lines in other directions, and along curves instead of straight lines – although we have not explored these conjectures.

Peaks in 1D can affect each other, through overlapping point-spread functions. Indeed, addressing such interaction is a primary motivation for invoking the double periodogram in the first place. In 2D the interactions are more complicated: mutual effects between periodicities, both near and far apart in frequency, play a significant role in the visualization and interpretation of double periodograms. Both single and double periodograms can be evaluated at any frequencies you choose. In 2D it is often convenient to make the two frequency arrays identical, although this is not necessary; for example one frequency range could center on a suspected periodicity, the other on its harmonic. To utilize super resolution the double periodogram must be oversampled significantly relative to the fundamental frequency of the data, $1/T$ cycles, or $2\pi/T$ radians, per unit time.

5.2. Sunspot Time Series

In spite of necessarily imperfect corrections for inhomogeneities due to evolving observational and measurement methodologies, the counts of sunspot numbers provides an instructive application of the double periodogram.

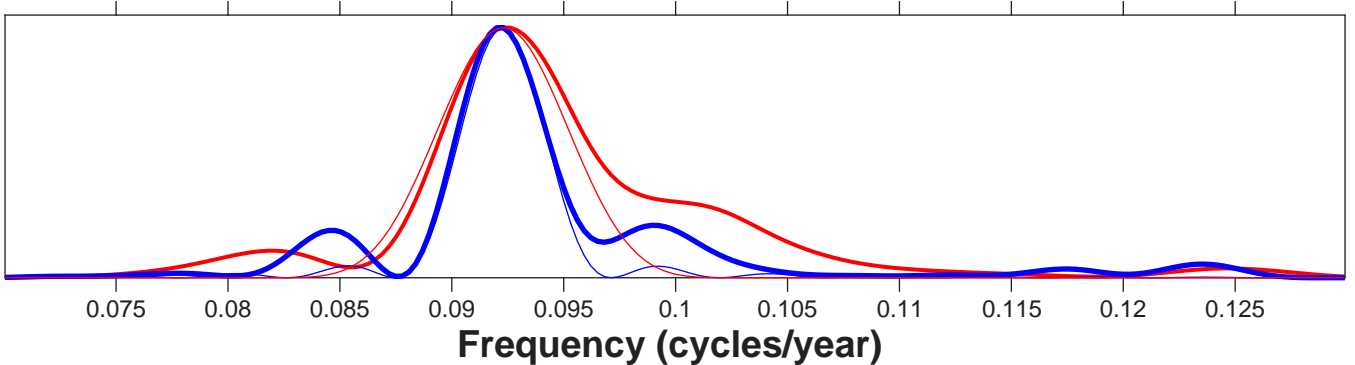


Figure 4. One dimensional LS periodograms of the sunspot time series, oversampled in frequency by a factor of 16: untapered and with a Slepian taper (thick blue and red lines, respectively). Window functions computed from the sample times as described in the footnote in Section 2.2 are thin lines in corresponding colors, shifted to coincide with the periodogram peaks.

Focusing on the frequency range corresponding to the \sim 11-year solar cycle, Figure 4 shows LSPs of just under 208 years of the daily sunspot number data from the World Data Center SILSO, Royal Observatory of Belgium, Brussels, <https://doi.org/10.24414/qnza-ac80> (Clette and Lefèvre, L. 2015), both plain and tapered with a first order Thomson-Slepian function with bandwidth parameter 2 (Thomson 1982; Springford, Eadie and Thomson 2020). The dominant peak at 0.0923 cycles/year (period 10.834 years) is flanked by asymmetric sidelobes, produced in part by the uneven sampling of the time series. The relative narrowness and symmetry of the spectral windows (the thin lines in the figure) suggests that the sidelobes in the periodograms are at least partially reflections of the complexities of the solar cycle.

Pursuing this suggestion, Fig. 5 displays evidence for multiple periodic components. The two distinct peaks in the double periodogram indicate resolution of the main feature in Fig. 4, hinted at there but not cleanly resolved. The separations here are marginally super resolution as such, since $\Delta\omega \approx 1.12 \omega_0$ is close to the fundamental. [Bretthorst \(1988\)](#) applied a variety of Bayesian periodogram-like techniques to astronomical data, including sunspot data available at the time. Given the difference in the data available then and now, his results are similar to ours.

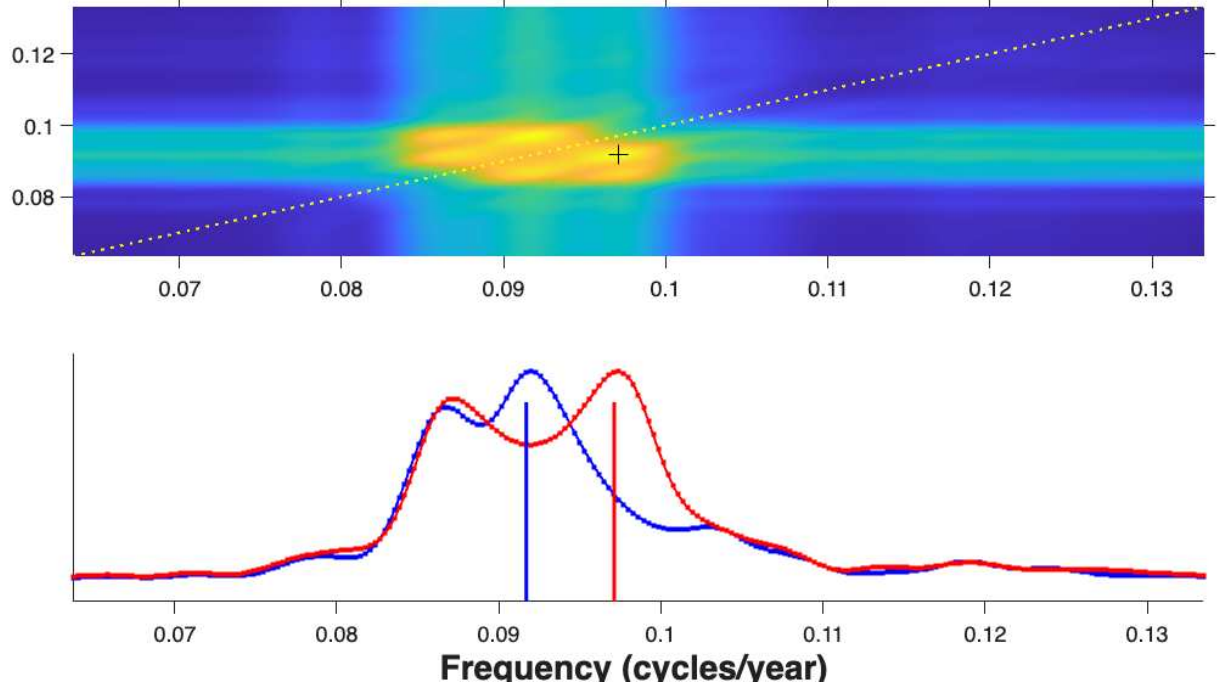


Figure 5. Top: DLSP for the sunspot number time series. The "+" symbol indicates the peak periodogram value at frequency coordinates (.0917 .0971), periods of 10.905 and 10.297 years, respectively. Bottom: Slices of the double periodogram passing through this peak: blue = vertical; red = horizontal. The two peak frequencies are marked with vertical lines.

5.3. The Pulsating White Dwarf WD J0135+5722

Let's investigate a more complicated case, to assess possible difficulties in a setting where multiple oscillations are simultaneously present. [De Geronimo et al. \(2025\)](#) discovered and analyzed the pulsating ultramassive white dwarf with the richest spectrum of oscillations. Figure 6 displays the LSP of the green filter time series kindly provided by these authors. Note the rich array of spectral peaks, with the potential of some structures lost due to overlap and limited resolution. To assess these possibilities, consider the double version of the same periodogram in Figure 7.

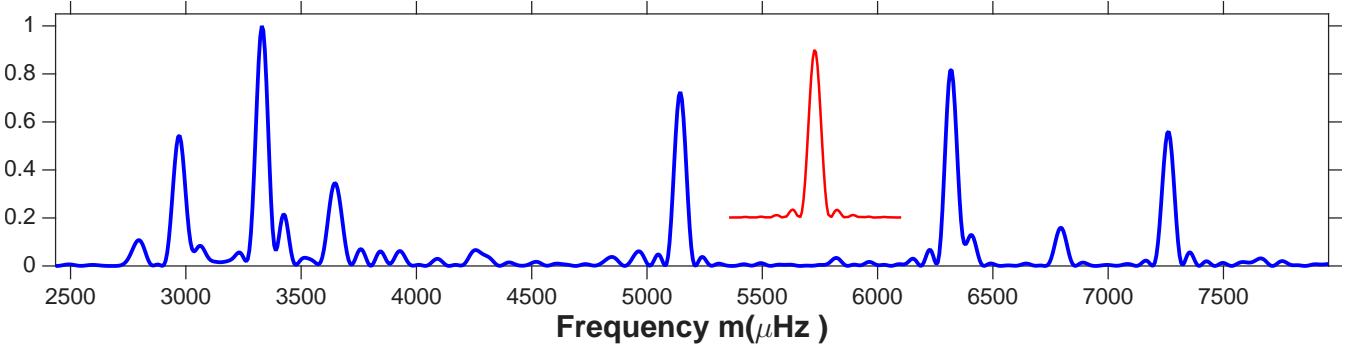


Figure 6. Blue: the LSP of the green time series of White Dwarf J0135+5722. Red: the corresponding window function.

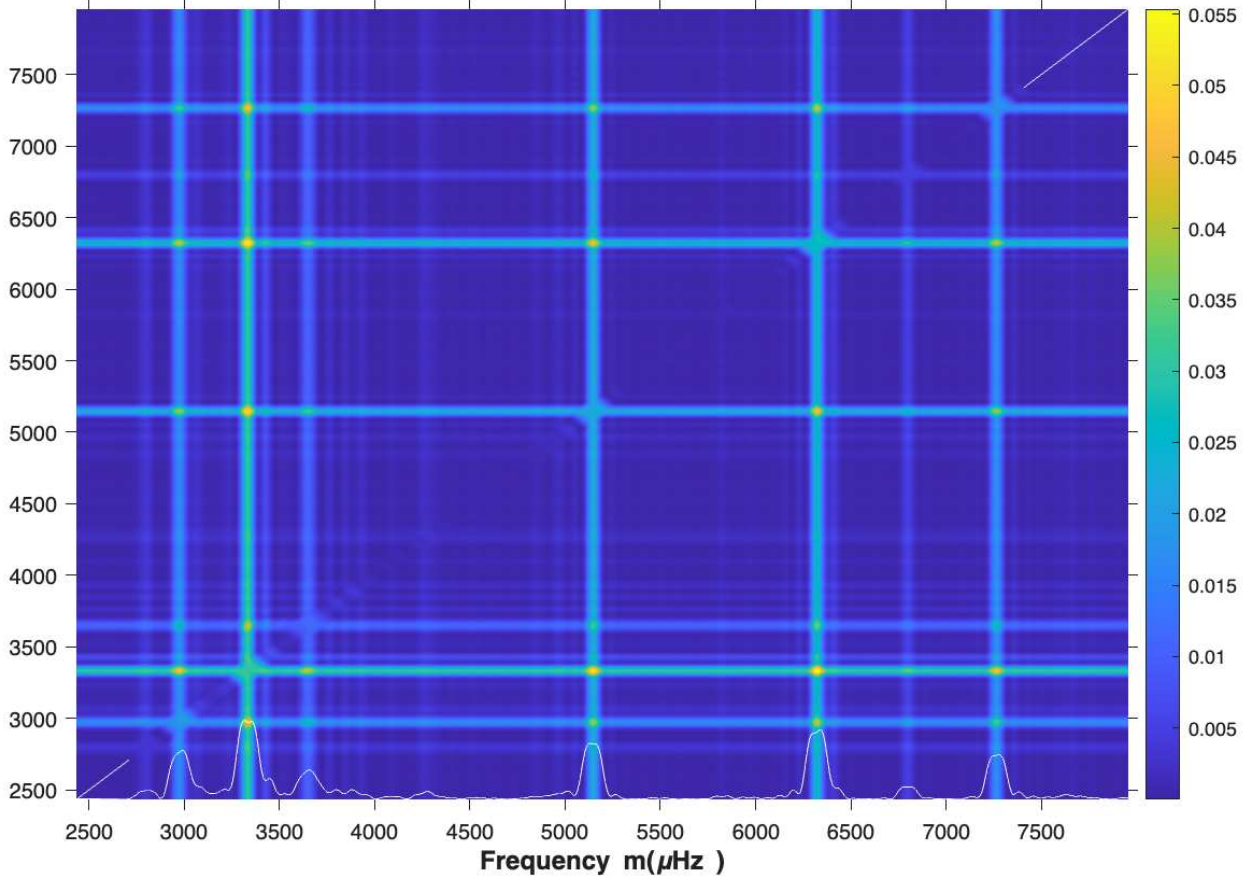


Figure 7. The DLSP periodogram $P(\omega_1, \omega_2)$ of the time series in the previous figure. A diagonal white line from the lower-left corner to the upper right, but interrupted between to avoid over-plotting features on the diagonal, is the locus $\omega_1 = \omega_2$. The white line at the bottom is a trace along the diagonal (scale arbitrary).

This figure contains a wealth of detailed information ... about individual oscillations and their pair-wise relationships. As with a 1D periodogram, local maxima (“peaks”) indicate discrete oscillations. The ones along the diagonal of the double periodogram are for the most part the same as those in the LSP. Pairs of oscillations appear as peaks offset from the diagonal in proportion to the difference in their frequencies. In fact, the amplitudes of these off-diagonal peaks are systematically larger than the diagonal ones. This is expected, since the off-diagonal likelihood contains contributions from two sinusoids, compared to just one on the diagonal. This effect can be seen roughly from the color scale, and is confirmed quantitatively: the distribution of the DLSP values (estimated as a simple histogram, not shown) has two peaks corresponding to values differing by a factor of two.

While providing a good view of the big picture in complicated situations like this, a double periodogram covering broad frequency intervals is moderately expensive. Focusing on a restricted part of the two-frequency plane suffices for many purposes. Because of the exchange symmetry $\omega_1 \leftrightarrow \omega_2$, analysis restricted to $\omega_2 \geq \omega_1$ can give a complete picture. Don’t forget that, as with any periodogram, you are free to evaluate it at any set of frequencies you want. Also, the periodogram for any subset is identical to that for the whole, as long as the frequency resolution is the same. E.g. a swath covering the diagonal only misses long-range interactions between components. The ranges of the frequency arrays do not need to be the same; a patch with ω_1 covering one periodicity and ω_2 covering another can be useful – e.g. in studying a periodicity and its harmonic(s).

In fact, we will now use small “postage stamp” subsets of the frequency plane to investigate the possibility that some of the peaks in the spectrum of WD J0135+5722 are composite. In particular, we ask whether it is possible to

separate them into two peaks, too close in frequency to be distinguished in Fig. 6. Following the above discussion, such peak-pairs are expected to appear as maxima near the diagonal, slightly offset from it because of the small frequency difference. Fig. 8 demonstrates this point, by injecting a pair of nearby (separation $R < 1$) sinusoids into the white dwarf time series data. The goal here is to study the resolution of close sinusoids in the presence of other, potentially interfering, signals. In order to avoid the injected signals falling on top of a major peak, we picked the interval around 3100μ Hz – amidst the peaks, but not to close to any one of them.

It can be seen in the figure that a pair of sinusoids at true separations of $R = 0.54$ and $R = 0.37$ are well resolved, but not for smaller R . At $R = 0.30$ there may be a hint of resolution, but the local maximum (red dot) has moved well away from the true point (black dot). The last panel is meant to characterize the DLSP of a single sinusoid embedded in a sea of other peaks. The black dot is actually close to the *local* maximum, but the maximum marked by the red dot (global for the range plotted) has been drawn off toward another peak; this underscores the caveat that determination of peaks-as-local-maxima has to be done carefully.

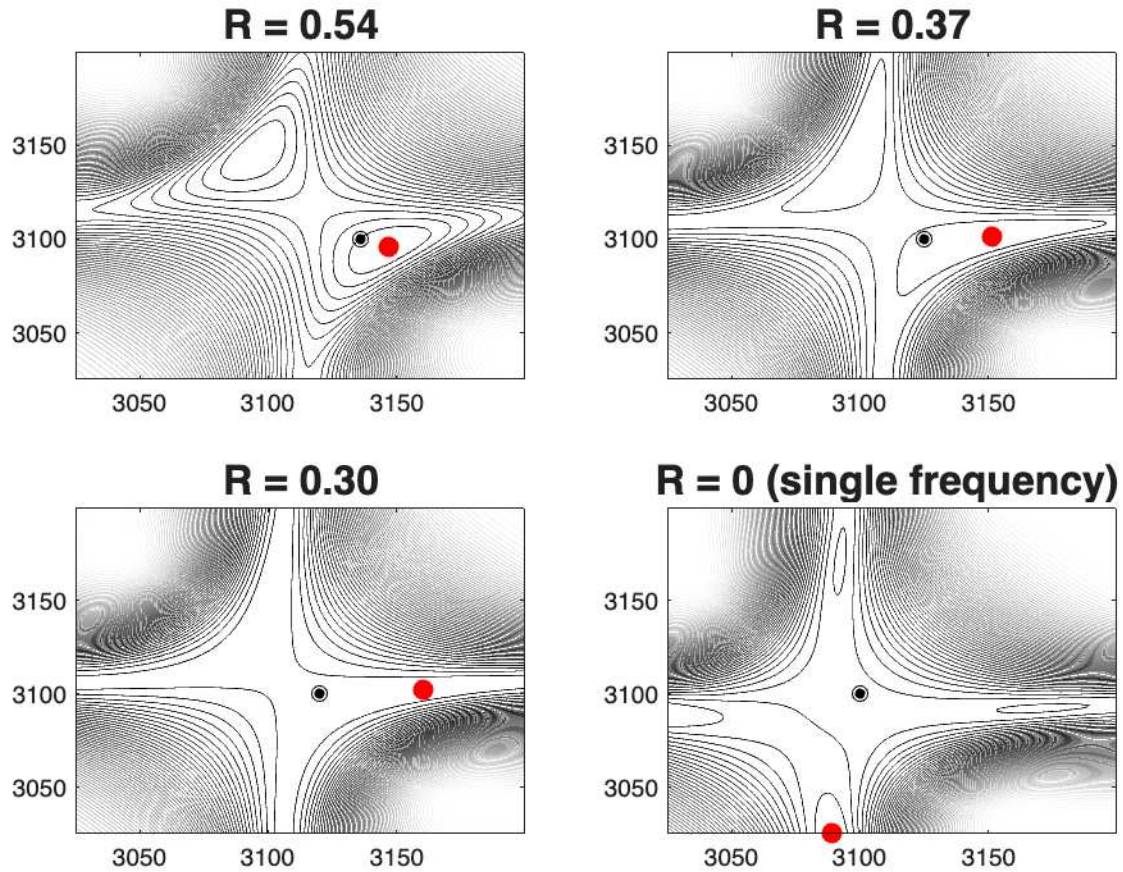


Figure 8. DLSPs for the WD J0135+5722 data injected with synthetic sinusoids: all 4 have one component at 3100μ Hz; in the first three panels, a synthetic second component (black dot) was injected, offset in frequency from this value by $\mathcal{R}_{\text{ayleigh}}$ times the fundamental ($= 67.2\mu$ Hz) for $\mathcal{R}_{\text{ayleigh}} = 0.54, 0.37$ and 0.30 . These components have equal amplitudes: the mean of the real time series. The 4th panel is for a single sinusoid at 3100μ , with no second component. Red dots are local maxima

The possibility of resolution of peaks in Figure 6 is addressed by comparing the DLSPs in Fig. 8 with that for a real peak in Fig. 9. This feature was selected for its relative isolation from other peaks. While the contours are slightly asymmetric, the fact that the local maximum falls exactly on the diagonal is clear evidence that this is a monochromatic oscillation, at the resolution level of a few tenths of a Rayleigh parameter R .

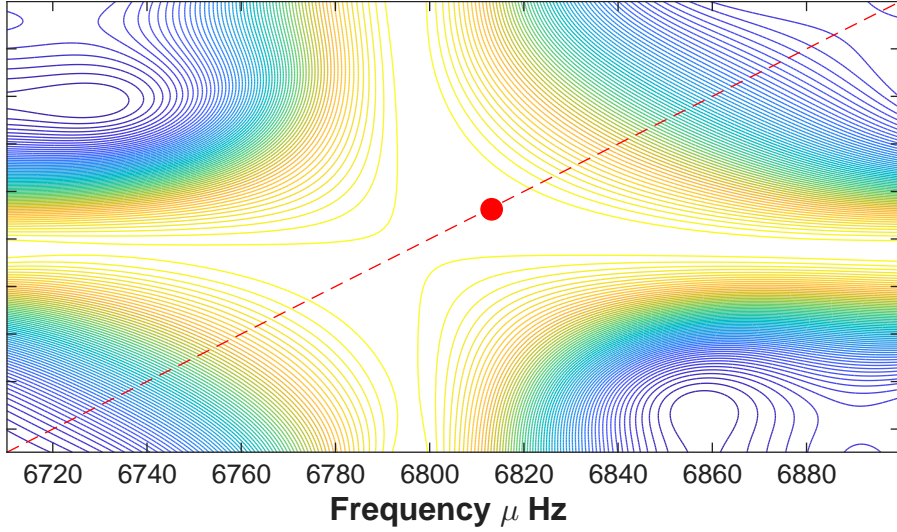


Figure 9. This is the DLSP localized to the peak in WD J0135+5722 at about $6800 \mu \text{Hz}$.

6. CONCLUSIONS

We provide explicit, turn-key algorithms for four types of double periodograms, functions of two frequencies, based on a model consisting of two independent sinusoids. These variants are derived by maximizing or marginalizing the likelihood, with or without the Lomb phase shift technique. In limited exploration, all four have similar behavior, including super resolution, as demonstrated with synthetic and real data. The appendix derives these algorithms as special cases of a more general one – for which we suggest the name *omnigram* – based on the [Bretthorst \(1988\)](#) model consisting of the sum of any number of arbitrary basis function.

Due to their flexibility and generality, omnigrams can be useful in a great variety of applications, as suggested by the following practical points:

- There is not just one single concept, “the” periodogram, rather a range with different sensitivities.
- Omnidograms are valid for most sequential data:
 - Point measurements, time-tagged events, time-to-spill data, etc.
 - The independent variable can be time, wavelength, spatial, etc.
 - The sampling can be even, even with gaps, jittered, arbitrarily uneven, etc.
- They can use basis functions of any kind, evaluated at any subset of the parameter hyperplane:
 - Sinusoids (classical periodograms)
 - Arbitrary functions
 - Arbitrary multiple parameterization.
- Analysis in sliding windows yields dynamic omnigrams (e.g. time-frequency distributions).
- Like classical periodograms, omnigrams can be useful even if the data model is not rigorously satisfied.
- Computation is straightforward and fast, since it involves elementary algebraic expressions.
- Especially useful are reconstructions of the maximum likelihood model from the optimal values of the component amplitudes returned by the algorithms.

These algorithms and the corresponding approach to power spectrum analysis should find broad use in any context where ordinary 1D periodograms have been applied, perhaps leading to new perspectives on periodicity detection and characterization. Here we have focused on the most straightforward context of resolving close frequencies, for

applications such as rotational or magnetic splitting in asteroseismology. Multi-period Keplerograms may be useful for studying multiple exoplanet systems. The case of widely separated frequencies is less clear. For coherent signals, as for a fundamental frequency and harmonics, relative phase information would be captured by a double periodogram.

Our analysis of sunspot data is offered as proof-of-concept. However, we note in passing: the period of 185 years, corresponding to the beat frequency between the two components identified in Figure 5, is roughly the time scale between the solar cycle’s historical minima; can these be simple interactions between periodic phenomena? This conjecture can be pursued with higher order periodograms, where we believe the basis of Eq. (F2) can be particularly useful.

Open issues include the development of a principled treatment of diagonal singularities, and this question: Is there a two-frequency function that can be regarded as a Fourier transform, the absolute-square of which is the DLSP?

ACKNOWLEDGMENTS

We are especially grateful to Tom Loredo for helpful discussions and access to unpublished notes, to Larry Bretthorst, Tony Readhead, David van Dyk, Vinay Kashyap, Daniel Fabrycky, Javier Pascual-Granado, and Victor Ramirez Delgado for useful comments, and to Francisco De Geronimo for providing the white dwarf data. Thanks to the anonymous referee for a helpful review that substantially improved the paper. We used ChatGPT for bibliographic assistance, but no artificially created text was used in the preparation of this manuscript.

APPENDIX

A. PERIODOGRAMS AND OMNIGRAMS

The construction of multi-frequency periodograms is greatly facilitated by symbolic algebra tools. We found it quite convenient to paste formulas generated, e.g. with MatLab's symbolic algebra system, directly into periodogram scripts. This almost completely automated process minimizes the risk of algebra errors in the rather complicated expressions.

Here we describe the generation of explicit algorithms for 4 variants: in short, maximizing or marginalizing likelihoods, with and without the Lomb orthogonalization procedure. Matlab and python code for the periodograms, scripts to construct them *ab initio*, and a test routine, will be found at the GitHub repository https://github.com/swagner-astro/double_periodogram. Readers are encouraged to generate their own scripts using the tools found there, for example using other basis functions, multifrequency models of other orders, or with other priors for the marginalization.

The notation such as in our Eq. (1), while standard in the literature, is not well suited to a symbolic algebraic approach, or to generalizations easily achieved with it – e.g. those explored in Bretthorst (1988). Accordingly, following Bretthorst's notation, we generalize the basic model to a linear combination of m arbitrary basis functions G_j with constant amplitudes B_j :

$$y_n = \sum_{j=1}^m \mathbf{B}_j \mathbf{G}_j(\mathbf{t}_n, \hat{\omega}_j) + \epsilon_n . \quad (\text{A.1})$$

Although Bretthorst (1988) presents detailed procedures for orthogonalizing basis functions, this is not necessary; indeed, the results seem more transparent without orthogonalization.

These basis functions depend on an arbitrary parameter, or possibly a set of parameters, denoted $\hat{\omega}_j$. Bretthorst comments that “... these parameters might be frequencies, chirp rates, decay rates, ...”, and has developed periodograms for amplitude modulated signals and chirps. Indeed, the $\hat{\omega}_j$ can be anything, enabling many possible statistical functions, *omnigrams*, for application to time series analysis. Note that some parameter subsets may be common to the m different functions – e.g. ω means the same thing in $G_1 = \cos(\omega t_n)$ and $G_2 = \sin(\omega t_n)$ – others may be specific to individual basis functions.

The models for the data and errors, y_n and ϵ_n , are unchanged from those of Section 3, so the log-likelihood satisfies

$$-2\log L = \sum_{n=1}^N \left(\frac{x_n - \sum_{j=1}^m B_j G_j(t_n, \hat{\omega}_j)}{\sigma_n} \right)^2 . \quad (\text{A.2})$$

Expanding the square yields this expression for the residual sum-of-squares:

$$Q = \sum_{n=1}^N x_n^2 - 2 \sum_{j=1}^m B_j \sum_{n=1}^N x_n G_j(t_n, \hat{\omega}_j) + \sum_{n=1}^N \left[\sum_{j=1}^m B_j G_j(t_n, \hat{\omega}_j) \right]^2 . \quad (\text{A.3})$$

Here we have implicitly incorporated the errors as statistical weights, multiplying x_n and $G_j(t_n, \hat{\omega}_j)$ for each value of n – not explicitly notated as such, but included in the expressions below. The first term can be discarded, since it is independent of the model parameters B_j . In the second term, the n -sums are inner products of the data vector and the basis functions, yielding terms linear in the B_j . Expanding the third term yields a quadratic form in the B_j , with the n -sums generating coefficients that are inner products of the basis functions $G_j(t_n)$ among themselves. We will see that maximizing or marginalizing this likelihood yields general expressions into which one simply needs to plug empirical values of these inner products to yield the corresponding periodograms.

Following Bretthorst's notation, the full expansion of this quadratic form, dropping the $\hat{\omega}_j$ symbols, for the two-component case, is

$$\begin{aligned} D(B_1, B_2, B_3, B_4) = & gg11 B_1^2 + gg22 B_2^2 + gg33 B_3^2 + gg44 B_4^2 \\ & - 2(dG1 B_1 + dG2 B_2 + dG3 B_3 + dG4 B_4) \\ & + 2(gg12 B_1 B_2 + gg13 B_1 B_3 + gg14 B_1 B_4 + gg23 B_2 B_3 + gg24 B_2 B_4 + gg34 B_3 B_4) \end{aligned} \quad (\text{A.4})$$

Here terms beginning gg are basis function inner products. E.g., with the basis of Equation (1), $gg12$ is $\sum_n \cos(\omega_1 t_n) \sin(\omega_1 t_n)$, $gg23$ is $\sum_n \sin(\omega_1 t_n) \cos(\omega_2 t_n)$, etc. Terms beginning dG are inner products with the data array, the appended numbers denoting which basis function is involved. The corresponding likelihood can be maximized or marginalized, eliminating the nuisance parameters B_j , yielding a function of the $\hat{\omega}_j$ valid for arbitrary basis functions. Here we outline the derivation of these double periodograms for an arbitrary fourfold basis. The results are valid for, but not limited to, the special case of the sinusoid basis in Eq. (1); this generality suggests the term *omnigram*.

B. THE MAXIMUM-LIKELIHOOD DOUBLE OMNIGRAM

The values of B_j maximizing D in Eq. (A.4), found by solving $\partial D / \partial B_j = 0$, are fractions, with the same denominator:

```

denominator =
- gg12^2*gg34^2 + gg33*gg44*gg12^2 - 2*gg44*gg12*gg13*gg23
+ 2*gg12*gg13*gg24*gg34 + 2*gg12*gg14*gg23*gg34
- 2*gg33*gg12*gg14*gg24 - gg13^2*gg24^2 + gg22*gg44*gg13^2
+ 2*gg13*gg14*gg23*gg24 - 2*gg22*gg13*gg14*gg34
- gg14^2*gg23^2 + gg22*gg33*gg14^2 + gg11*gg44*gg23^2
- 2*gg11*gg23*gg24*gg34 + gg11*gg33*gg24^2
+ gg11*gg22*gg34^2 - gg11*gg22*gg33*gg44

```

For convenience, we organize the numerators by collecting terms involving inner products dG_j of the data with each basis function $G_j(t_n)$ separately, yielding

$$B_j = (QdG1*dG1+QdG2*dG2+QdG3*dG3+QdG4*dG4) / \text{denominator}$$

for each, but with different values of the Q terms as follows ($j = 1, 2, 3, 4$):

$$\begin{aligned}
QdG1 &= gg22*gg34^2+gg24^2*gg33+gg23^2*gg44-2*gg23*gg24*gg34-gg22*gg33*gg44 \\
QdG2 &= gg13*gg24*gg34-gg12*gg34^2+gg14*gg23*gg34-gg14*gg24*gg33-gg13*gg23*gg44+gg12*gg33*gg44 \\
QdG3 &= -(gg13*gg24^2-gg14*gg23*gg24-gg12*gg24*gg34+gg14*gg22*gg34+gg12*gg23*gg44-gg13*gg22*gg44) \\
QdG4 &= gg13*gg23*gg24-gg14*gg23^2+gg12*gg23*gg34-gg12*gg24*gg33-gg13*gg22*gg34+gg14*gg22*gg33 \\
QdG1 &= gg13*gg24*gg34-gg12*gg34^2+gg14*gg23*gg34-gg14*gg24*gg33-gg13*gg23*gg44+gg12*gg33*gg44 \\
QdG2 &= gg11*gg34^2+gg14^2*gg33+gg13^2*gg44-2*gg13*gg14*gg34-gg11*gg33*gg44 \\
QdG3 &= gg13*gg14*gg24-gg14^2*gg23+gg12*gg14*gg34-gg11*gg24*gg34-gg12*gg13*gg44+gg11*gg23*gg44 \\
QdG4 &= -(gg13^2*gg24-gg13*gg14*gg23-gg12*gg13*gg34+gg12*gg14*gg33+gg11*gg23*gg34-gg11*gg24*gg33) \\
QdG1 &= -(gg13*gg24^2-gg14*gg23*gg24-gg12*gg24*gg34+gg14*gg22*gg34+gg12*gg23*gg44-gg13*gg22*gg44) \\
QdG2 &= gg13*gg14*gg24-gg14^2*gg23+gg12*gg14*gg34-gg11*gg24*gg34-gg12*gg13*gg44+gg11*gg23*gg44 \\
QdG3 &= gg11*gg24^2+gg14^2*gg22+gg12^2*gg44-2*gg12*gg14*gg24-gg11*gg22*gg44 \\
QdG4 &= gg12*gg13*gg24-gg12^2*gg34+gg12*gg14*gg23-gg13*gg14*gg22-gg11*gg23*gg24+gg11*gg22*gg34 \\
QdG1 &= gg13*gg23*gg24-gg14*gg23^2+gg12*gg23*gg34-gg12*gg24*gg33-gg13*gg22*gg34+gg14*gg22*gg33 \\
QdG2 &= -(gg13^2*gg24-gg13*gg14*gg23-gg12*gg13*gg34+gg12*gg14*gg33+gg11*gg23*gg34-gg11*gg24*gg33) \\
QdG3 &= gg12*gg13*gg24-gg12^2*gg34+gg12*gg14*gg23-gg13*gg14*gg22-gg11*gg23*gg24+gg11*gg22*gg34 \\
QdG4 &= gg11*gg23^2+gg13^2*gg22+gg12^2*gg33-2*gg12*gg13*gg23-gg11*gg22*gg33
\end{aligned}$$

The final value of the periodogram is obtained by inserting these values into Eq. (A.4). Note that the maximum likelihood values of the amplitude parameters B_j are an automatic byproduct of this computation; in the case of a sinusoidal basis, they are useful for estimating the amplitudes and phases of two components.

C. THE MARGINALIZED-LIKELIHOOD DOUBLE OMNIGRAM

We follow the idea of [Bretthorst \(1988\)](#) to marginalize the likelihood corresponding to Eq. (A.3) with respect to the amplitudes B_j . This approach has the advantage that various prior distribution functions for these nuisance parameters

can be invoked. Gaussian priors are particularly easy to incorporate. However, the procedure detailed here uses the same flat prior as Brethorst, in which case there is a formal equivalence between Bayesian and maximum-likelihood regression. Practical differences implemented in our analysis include automatic determination of the amplitude parameters in the former, and the fact that the latter utilizes the average over the full posterior, not just its maximum as in the former.

The marginalization integrals

$$P(\{\hat{\omega}_j\}) = \int_{-\infty}^{\infty} \cdots \int_{-\infty}^{\infty} e^Q dB_1 dB_2 \dots dB_m, \quad (\text{C.1})$$

with Q defined in Equ. (A.4), can be evaluated with m -fold application of the famous Gaussian integral

$$\int_{-\infty}^{\infty} e^{-(Ax^2+Bx+C)} dx = \sqrt{\frac{\pi}{A}} e^{(B^2/4A)-C}. \quad (\text{C.2})$$

Applied to $\int_{-\infty}^{\infty} e^Q dB_1$, since there A is a constant (gg11), the factor $\sqrt{\frac{\pi}{A}}$ is a constant, and the factor $e^{(B^2/4A)-C}$ is the exponential of a quadratic form in the remaining variables B_2, B_3, \dots . Proceeding iteratively, this integral can be carried out to any order, yielding the fully marginalized posterior as the product of the accumulated $\sqrt{\frac{\pi}{A}}$ factors and the final value of $e^{(B^2/4A)-C}$. A script in the GitHub repository carries out the details of this iterative procedure, using basic symbolic algebra functions, as follows:

$$\begin{aligned} RC &= \text{coeffs}(Q, B_j) \\ A &= RC(3) \quad B = RC(2) \quad C = RC(1) \\ R &= -(B^2/(4A)) + C \end{aligned} \quad (\text{C.3})$$

where the function `coeffs` returns polynomial coefficients as indicated. The result for the case of a general fourfold basis again has a denominator depending on only the basis functions,

```
denominator = (- gg12^2*gg34^2 + gg33*gg44*gg12^2
- 2*gg44*gg12*gg13*gg23 + 2*gg12*gg13*gg24*gg34
+ 2*gg12*gg14*gg23*gg34 - 2*gg33*gg12*gg14*gg24
- gg13^2*gg24^2 + gg22*gg44*gg13^2 + 2*gg13*gg14*gg23*gg24
- 2*gg22*gg13*gg14*gg34 - gg14^2*gg23^2 + gg22*gg33*gg14^2
+ gg11*gg44*gg23^2 - 2*gg11*gg23*gg24*gg34 + gg11*gg33*gg24^2
+ gg11*gg22*gg34^2 - gg11*gg22*gg33*gg44)
```

and this numerator, involving the terms from the inner products of basis functions with the data x_n :

```
numerator = QdG1p2*dG1^2 + QdG1dG2*dG1*dG2 + QdG1dG3*dG1*dG3
+ QdG1dG4*dG1*dG4 + QdG2p2*dG2^2 + QdG2dG3*dG2*dG3
+ QdG2dG4*dG2*dG4 + QdG3p2*dG3^2 + QdG3dG4*dG3*dG4
+ QdG4p2*dG4^2
```

in terms of

```
QdG1p2=gg22*gg34^2+gg24^2*gg33+gg23^2*gg44-2*gg23*gg24*gg34-gg22*gg33*gg44
QdG1dG2=2(gg13*gg24*gg34-gg12*gg34^2+gg14*gg23*gg34-gg14*gg24*gg33-gg13*gg23*gg44+gg12*gg33*gg44)
QdG1dG3=-2(gg13*gg24^2-gg14*gg23*gg24-gg12*gg24*gg34+gg14*gg22*gg34+gg12*gg23*gg44-gg13*gg22*gg44)
QdG1dG4=2(gg13*gg23*gg24-gg14*gg23^2+gg12*gg23*gg34-gg12*gg24*gg33-gg13*gg22*gg34+gg14*gg22*gg33)
QdG2p2=gg11*gg34^2+gg14^2*gg33+gg13^2*gg44-2*gg13*gg14*gg34-gg11*gg33*gg44
QdG2dG3=2(gg13*gg14*gg24-gg14^2*gg23+gg12*gg14*gg34-gg11*gg24*gg34-gg12*gg13*gg44+gg11*gg23*gg44)
QdG2dG4=-2(gg13^2*gg24-gg13*gg14*gg23-gg12*gg13*gg34+gg12*gg14*gg33+gg11*gg23*gg34-gg11*gg24*gg33)
QdG3p2=gg11*gg24^2+gg14^2*gg22+gg12^2*gg44-2*gg12*gg14*gg24-gg11*gg22*gg44
QdG3dG4=2(gg12*gg13*gg24-gg12^2*gg34+gg12*gg14*gg23-gg13*gg14*gg22-gg11*gg23*gg24+gg11*gg22*gg34)
QdG4p2=gg11*gg23^2+gg13^2*gg22+gg12^2*gg33-2*gg12*gg13*gg23-gg11*gg22*gg33
```

In addition, the accumulated “A factors” are

```
A_fac = gg12^2*gg34^2 - gg33*gg44*gg12^2 + 2*gg44*gg12*gg13*gg23
      - 2*gg12*gg13*gg24*gg34 - 2*gg12*gg14*gg23*gg34 + 2*gg33*gg12*gg14*gg24
      + gg13^2*gg24^2 - gg22*gg44*gg13^2 - 2*gg13*gg14*gg23*gg24
      + 2*gg22*gg13*gg14*gg34 + gg14^2*gg23^2 - gg22*gg33*gg14^2
      - gg11*gg44*gg23^2 + 2*gg11*gg23*gg24*gg34 - gg11*gg33*gg24^2
      - gg11*gg22*gg34^2 + gg11*gg22*gg33*gg44
```

and the final expression for this Bayesian omnigram is

```
P = (numerator / denominator) - 0.5 * log( A_fac ),
```

evaluated as a function of the free parameter(s) $\hat{\omega}_j$.

D. INNER PRODUCTS FOR THE TWO-SINUSOID MODEL

The inner products for both the maximum and marginalized likelihood cases are the same. As emphasized below, these above formulas are valid for any basis functions, but it may be instructive to display the inner products explicitly for our basic special case of two sinusoids, as in Eq. (1), with the notation `ww_11` standing for ω_1 , etc., and `xx_vec` and `tt_vec` the data samples, this is:

```
cos_11_vec = cos( ww_11 * tt_vec )
sin_11_vec = sin( ww_11 * tt_vec )
cos_22_vec = cos( ww_22 * tt_vec )
sin_22_vec = sin( ww_22 * tt_vec )

gg11 = sum( wt_vec * abs( cos_11_vec ).^ 2)
gg22 = sum( wt_vec * abs( sin_11_vec ).^ 2)
gg12 = sum( wt_vec * cos_11_vec * sin_11_vec )

dG1 = sum( wt_vec * xx_vec * cos_11_vec )
dG2 = sum( wt_vec * xx_vec * sin_11_vec )

gg33 = sum( wt_vec * abs( cos_22_vec ).^ 2)
gg44 = sum( wt_vec * abs( sin_22_vec ).^ 2)
gg34 = sum( wt_vec * cos_22_vec * sin_22_vec )

dG3 = sum( wt_vec * xx_vec * cos_22_vec )
dG4 = sum( wt_vec * xx_vec * sin_22_vec )

gg13 = sum( wt_vec * cos_11_vec * cos_22_vec )
gg24 = sum( wt_vec * sin_11_vec * sin_22_vec )

gg14 = sum( wt_vec * cos_11_vec * sin_22_vec )
gg23 = sum( wt_vec * sin_11_vec * cos_22_vec )
```

E. OMNIGRAMS WITH THE LOMB PHASE SHIFT TERM

The simplification yielded by the orthogonalization introduced by Lomb (1976) is easily implemented by discarding the inner products corresponding to the basis functions to be made orthogonal from the likelihood in Eq. (A.4). For

the standard double sinusoid case these are `gg12` and `gg34` (but not any terms crossing between the components, such as `gg13`, `gg14`, etc., the removal of which would presumably cripple the main property of the omnigram). Slightly offsetting this simplification is the need to pre-compute the Lomb phase shift, e.g. for the sinusoidal basis:

$$\theta_{[1,2]} = \frac{1}{2} \arctan \frac{\sum_n w_n \sin 2\omega_{[1,2]} t_n}{\sum_n w_n \cos 2\omega_{[1,2]} t_n}, \quad (\text{E1})$$

and then changing the arguments of the `sin` and `cos` functions to `ww_11 * tt_vec - theta`, etc. The resulting omnigram formulas are different, and cannot be obtained from those shown above by deleting the corresponding terms; they are contained in the GitHub repository.

The values a_1, b_1, a_2 , and b_2 are automatic, useful by-products of the computation. For any periodogram utilizing the Lomb orthogonalization procedure, they are coefficients of the phase-shifted sinusoids. To refer them to the actual sinusoids, they need to be corrected as follows. If $\omega_{[1,2]}\tau_{[1,2]}$ are the Lomb phase shifts, at any frequency in any of the relevant periodograms, then for either of the two components:

$$a_{[1,2]}(\text{corrected}) = a_{[1,2]} \sin(\omega_{[1,2]}\tau_{[1,2]}) + b_{[1,2]} \cos(\omega_{[1,2]}\tau_{[1,2]}) \quad (\text{E2})$$

$$b_{[1,2]}(\text{corrected}) = b_{[1,2]} \sin(\omega_{[1,2]}\tau_{[1,2]}) - a_{[1,2]} \cos(\omega_{[1,2]}\tau_{[1,2]}) \quad (\text{E3})$$

There is one caveat for both types of omnigrams. The expressions derived above are singular for the degenerate case $\omega_1 = \omega_2$. Typically the values of double periodogram vary smoothly enough near this locus to warrant simple interpolation across this singularity. In the examples in the main text, each pixel on the diagonal was computed as the average of the 6 adjacent off-diagonal values (2 at the endpoints). The sampling can always be made fine enough for this approximation to be valid, but a more principled resolution of these singularities would be valuable.

This orthogonalization procedure may or make not make sense for alternative basis functions, to be discussed next.

F. ALTERNATIVE BASIS FUNCTIONS

Any linear time series model implicitly defines a basis set, consisting of the functions in the linear form. For example, the Fourier basis implicit in Eq. (1) is a natural choice in the search for periodic signals. But other bases are useful in a variety of applications. For any basis, Appendices B and C develop general omnigram formulas, and Appendix D demonstrates “plugging” sinusoidal basis functions into them; exactly the same procedure applies for any basis.

We list a few examples from the unlimited possibilities:

- For signals that are periodic, but more complicated than sinusoidal in form, this one-frequency periodogram based on the model

$$y_n = a_1 \cos(\omega t_n) + b_1 \sin(\omega t_n) + a_2 \cos(2\omega t_n) + b_2 \sin(2\omega t_n), \quad (\text{F1})$$

may be useful, and perhaps extended to even higher harmonics.

- A basis consisting of the absolute values of the standard `sin` and `cos` functions, e.g.

$$y_n = |a_1 \cos(\omega t_n)| + |b_1 \sin(\omega t_n)|, \quad (\text{F2})$$

may be useful for count data, e.g. sunspot number time series.

- This basis implied by a model discussed by [Baluev \(2013a\)](#), namely

$$\begin{aligned} y_n = & a_1 \cos((\omega_1 + \omega_2)t_n) \cos((\omega_1 - \omega_2)t_n) \\ & + b_1 \sin((\omega_1 + \omega_2)t_n) \cos((\omega_1 - \omega_2)t_n) \\ & + a_2 \cos((\omega_1 + \omega_2)t_n) \sin((\omega_1 - \omega_2)t_n)/(\omega_2 - \omega_1) \\ & + b_2 \sin((\omega_1 + \omega_2)t_n) \sin((\omega_1 - \omega_2)t_n)/(\omega_2 - \omega_1), \end{aligned} \quad (\text{F3})$$

may have useful behavior at or near the $\omega_1 = \omega_2$ singularity.

- Bretthorst (1988) studied a chirp model of the form

$$y_n = a \cos(\omega t_n + \alpha t_n^2) + b \sin(\omega t_n + \alpha t_n^2) + c, \quad (\text{F4})$$

where the *chirp rate* α is the time rate of change of the frequency of this quasi-sinusoidal signal, which has time dependent *instantaneous amplitude* and *instantaneous phase*, as well as harmonic relationships and amplitude modulations for similar signals.

- Loredo, Berger, Chernoff, Clyde, and Liu (2010) derived periodogram-like quantities based on Kepler orbits of exoplanets, with the goal of improving sensitivity to eccentric orbits, e.g. a *Kepler-o-Gram* depending on orbital period, eccentricity, and mean anomaly at a fiducial time.
- Leaving the frequency domain, consider analysis of time-domain flares, with basis functions representing profile shape and location in time. Fig. F1 demonstrates an example of this *deconvolution* problem, namely the resolution of two closely spaced exponential flares by an omnigram using basis functions

$$\begin{aligned} F(t_n | \tau_{1,2}, a) &= e^{a(t_n - \tau_{1,2})} & t_n \geq \tau_{1,2} \\ &= 0 & \text{otherwise,} \end{aligned} \quad (\text{F5})$$

with τ_1 and τ_2 the times, and a the (same) decay constant for the flares. This is essentially a first order autoregressive process model. In view of the flares' closeness in time, as well as the added noise, this would be a very hard problem for conventional deconvolution methods; hence this is *super time resolution*, as remarkable as the super frequency resolution demonstrated in Section 4. This example result is offered as proof-of-concept only; the estimate of the decay constant is not especially robust with respect to the parameters, and deconvolution with different decay constants for the components is problematic.

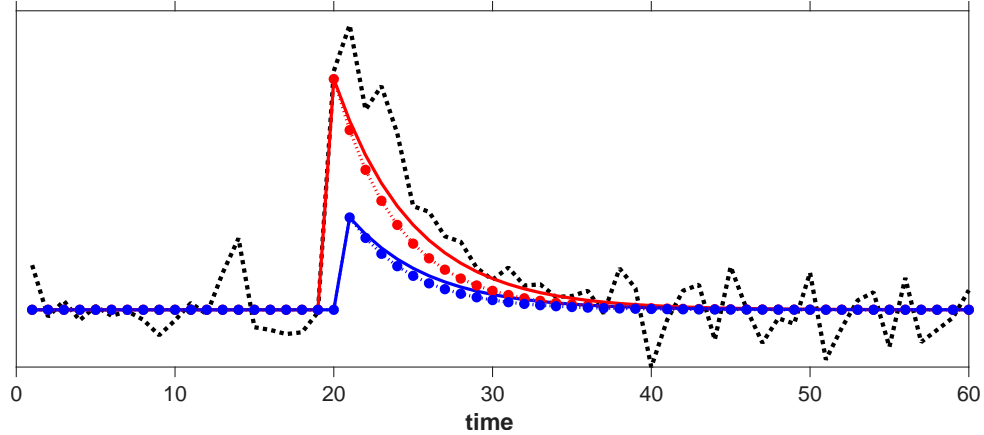


Figure F1. Omnigram Deconvolution of Overlapping Flares. Red and blue lines: two synthetic instantaneous-rise-exponential-decay flares, with the same decay coefficient, separated by one unit of time and with amplitudes 1 and 0.4. Dotted black line: the sum of these with added Gaussian noise of amplitude 0.1. Red and blue dots: profiles recovered by finding the omnigram peak.

G. SUGGESTED TERMINOLOGY

In the examples presented in this paper the four periodogram flavors give almost identical results. We have not explored differences between them, but it seems reasonable to provide code for all of them, and to recommend the terminology in Table G1, meant to convey the principles behind the periodograms, and perhaps forestall terminological confusion. All of these are special cases of *omnigrams* with their arbitrary number of arbitrary basis functions.

Table G1. Double Periodograms $P(\omega_1, \omega_2)$

Name:		Method	Lomb Phase Term?
Double Schuster Periodogram	DSP	Max-Likelihood	N
Double Lomb-Scargle Periodogram	DLSP	Max-Likelihood	Y
Double Brethorst-Schuster Periodogram	DBSP	Max-Posterior	N
Double Brethorst-Lomb-Scargle Periodogram	DBLSP	Max-Posterior	Y

REFERENCES

Baluev, R. 2013, Detecting multiple periodicities in observational data with the multi-frequency periodogram. I. Analytic assessment of the statistical significance, *MNRAS*, 436, 807–818

Baluev, R. 2013, Detecting multiple periodicities in observational data with the multifrequency periodogram—II. Frequency Decomposer, a parallelized time-series analysis algorithm, *Astronomy and Computing*, 3–4, 50–57.

Baluev, R. 2015, Keplerian periodogram for doppler exoplanet detection: optimized computation and analytic significance thresholds, *Mon. Not. R. Astron. Soc.*, 446, 1478–1492

Barning, F. J. M., 1963, The numerical analysis of the light-curve of 12 Lacertae, *Bulletin of the Astronomical Institutes of the Netherlands*, 17, 22.

Bretthorst, G. L. 1988, Bayesian Spectrum Analysis and Parameter Estimation, No. 48 in *Lecture Notes in Statistics*, Eds. Berger, J. et al., <https://bayes.wustl.edu/glb/book.pdf> (special permission to make the electronic version available freely was given by the publisher in 1997).

Bretthorst, G. L. 2000, Frequency Estimation and Generalized Lomb-Scargle Periodograms, *Statistical Challenges in Astronomy in 2000*, 309–329, Springer, New York, NY. 1988

Bretthorst, G. L. 2001, Generalizing the Lomb-Scargle periodogram—the non-sinusoidal case *AIP Conf. Proc.* 568, 246–251, <https://doi.org/10.1063/1.1381889>

Bretthorst, G. L. 2001, Generalizing the Lomb-Scargle periodogram, *AIP Conf. Proc.* 568, 241–245 (2001) <https://doi.org/10.1063/1.1381888>

Bretthorst, G. L. 2003, *AIP Conf. Proc.* 659, 3–22 (2003) <https://doi.org/10.1063/1.1570531>

Bretthorst, G. L. 2008, Nonuniform sampling: Bandwidth and Aliasing, *Concepts in Magnetic Resonance Part A*, 32A(6), 417–435. Reprinted from *Maximum Entropy and Bayesian Methods in Science and Engineering*, 567, 1–18, American Institute of Physics.

Clette, F. and Lefèvre, L. 2015, Published by WDC SILSO - Royal Observatory of Belgium. <https://doi.org/10.24414/qnza-ac80>

Dawson, R. and Fabrycky, D. 2010, Radial velocity planets de-aliased: a new short period for super-earth 55 Cnc e *ApJ* 722, 937

De Geronimo, F., Uzundag, M., Rebassa-Mansergas, A., Brown, A., Kilic, M., Corsico, A., Jewett, G., and Moss, A. 2025, Discovery of the richest pulsating ultra-massive white dwarf, [arXiv:2501.13661](https://arxiv.org/abs/2501.13661),

Gilliland, R. and Baliunas, S. 1987, *ApJ* 314, 766 lenoirviroloir.org/

Lenoir, G. and Crucifix, M. 2018, A general theory on frequency and time-frequency analysis of irregularly sampled time series based on projection methods – Part 1: Frequency analysis, *Nonlin. Processes Geophys.*, 25, 145–173

Lomb, N., 1976, Least-squares frequency analysis of unequally spaced data, *Astrophysics and Space Science*, 39, 447–462

Loredo, T. 2001, Bayesian Harmonic Analysis for Audio Testing and Measurement, *Audio Engineering Society Convention Number 111*, Paper Number 5447, hosting.astro.cornell.edu/~loredo/bayes/tj1.html

Loredo, T., Berger, J., Chernoff, D., Clyde, M., and Liu, B. 2010, Bayesian Methods for Analysis and Adaptive Scheduling of Exoplanet Observations, *Statistical Methodology* 9, 101–114

A Search for Supermassive Black Hole Binary Candidates in 46-Year Radio Light Curves of 83 Blazars, preprint 2510.23103

Mortier, A., Farim J., Correia, C., Santerne, A., Santos, N. 2015, BGLS: A Bayesian formalism for the generalized Lomb-Scargle periodogram, *A. and A.* 573, 101

Olspert, N., Pelt, J., Käpylä, M., Lehtinen, J. 2018, Estimating activity cycles with probabilistic methods I. Bayesian generalised Lomb-Scargle periodogram with trend, *A. and A.* 615, A111

The Rayleigh Criterion: Resolution Limits of Astronomical Periodograms Ramirez Delgado, V., Caicedo Vivas, J., Dodson-Robinson, S., and C. Haley, C. 2025, *PASP*, 137, 25 [arXiv:2506.20864](https://arxiv.org/abs/2506.20864)

Scargle, J. 1982, Studies in Astronomical Time Series Analysis: II. Statistical Aspects of Spectral Analysis of Unevenly Spaced Data, *ApJ*, 263, 835–853.

Scargle, J. 1989, Studies in astronomical time series analysis. III. Fourier Transforms, Autocorrelation Functions, and Cross-Correlation Functions of Unevenly Spaced Data. *ApJ*, 343, 874–887

Schuster, A., 1898, "On the investigation of hidden periodicities with application to a supposed 26 day period of meteorological phenomena" *Terrestrial Magnetism*, 3, 13–41.

Seilmayer, M., Wondrak, T., and Garcia, F., Multivariate Frequency and Amplitude Estimation for Unevenly Sampled Data Using and Extending the Lomb-Scargle Method, *Sensors*, 25, 6535.

Springford, A., Eadie, G., and Thomson, D. 2020, Improving the Lomb-Scargle Periodogram with the Thomson Multitaper, *Astronomical Journal*, 159, 205

Thomson, D. J 1982, Spectrum estimation and harmonic analysis. *Proceedings of the IEEE*, 70, 1055–1096

VanderPlas, J. 2018, Understanding the Lomb-Scargle Periodogram, *ApJS*, 236.

Vaughan, S. 2010, A Bayesian test for periodic signals in red noise *MNRAS* 402, 30

Vio, R. , Andreani, P, and Biggs, A. 2010, Unevenly-sampled signals: a general formalism for the Lomb-Scargle periodogram, *A&A* 519, A85

Zechmeister, M. and Kürster, 2009, The generalised Lomb-Scargle periodogram. A new formalism for the floating-mean and Keplerian periodograms, *Astronomy and Astrophysics*, 496, 577